IEEE Access
Multidisciplinary | Rapid Review | Open Access Journal

Received March 1, 2022, accepted March 13, 2022, date of publication March 17, 2022, date of current version March 25, 2022.

Digital Object Identifier 10.1109/ACCESS.2022.3160476

Dual-Band Circularly Polarized Omni-Directional Biconical Antenna With Double-Circular Parallelepiped Elements for WLAN Applications

PISIT JANPANGNGERN[1], DANAI TORRUNGRUENG[2], (Senior Member, IEEE), MONAI KRAIRIKSH[1], (Senior Member, IEEE), AND CHUWONG PHONGCHAROENPANICH[1], (Member, IEEE)

[1]School of Engineering, King Mongkut's Institute of Technology Ladkrabang, Bangkok 10520, Thailand
[2]Research Center of Innovation Digital and Electromagnetic Technology, Department of Teacher Training in Electrical Engineering, Faculty of Technical Education, King Mongkut's University of Technology North Bangkok, Bangkok 10800, Thailand

Corresponding author: Chuwong Phongcharoenpanich (chuwong.ph@kmitl.ac.th)

This work was supported in part by the King Mongkut's Institute of Technology Ladkrabang under Grant 2564-02-01-006, in part by the King Mongkut's University of Technology North Bangkok under Contract KMUTNB-64-KNOW-12, and in part by the Royal Golden Jubilee Ph.D. Program of the Thailand Research Fund (RGJ-TRF) under Grant PHD/0170/2560.

ABSTRACT This research proposes a novel dual-band (2.45/5.80 GHz) omnidirectional circularly polarized (CP) biconical antenna with double-circular parasitic parallelepiped elements for wireless local area network (WLAN) applications. The proposed dual-band CP antenna scheme consisted of a biconical radiating structure surrounded by inner- and outer-circular parallelepiped elements that convert linearly polarized electric fields into CP fields. Simulations were performed to optimize the antenna parameters, and an antenna prototype was fabricated and experiments were conducted. The measured impedance bandwidths (IBWs) were 44.4% (1.84 – 2.89 GHz) and 4.56% (5.73 – 5.99 GHz) for the lower- (2.4 GHz) and upper-frequency (5.80 GHz) bands, respectively. The corresponding 3-dB axial ratio bandwidths (ARBWs) were 11.22% (2.27 – 2.54 GHz) and 10.49% (5.6 – 6.2 GHz). The radiation patterns of the dual-band antenna scheme were omnidirectional left-hand circular polarization, with the measured antenna gains of 3.2 dBic and 8.5 dBic at 2.45 and 5.80 GHz, respectively. The simulated and measured results were reasonably agreeable. Despite the narrow IBW and ARBW for the upper-frequency band, the bandwidths adequately covered the target upper frequency band, rendering the proposed CP omnidirectional biconical antenna scheme operationally suitable for WLAN applications. Furthermore, the novelty of this research lies in the use of a biconical radiating structure augmented with double-circular parasitic parallelepiped elements to realize circular polarization for dual-band WLAN applications.

INDEX TERMS Circular polarization, biconical antenna, omnidirectional radiation pattern, WLAN applications.

I. INTRODUCTION

The advancement in modern wireless communication technology, including WLAN (2.4–2.48, 5.15–5.35, 5.725–5.875 GHz), WiMAX (2.5–2.69, 3.4–3.69, 5.25–5.85 GHz), Wi-Fi (2.4–2.485, 5.15–5.85 GHz), and Bluetooth (2.4–2.5 GHz), has fueled the demand for versatile antennas with circular polarization characteristics.

The advantages of circularly polarized (CP) antennas include versatility, lower multipath loss, and higher penetration, unlike the linearly polarized (LP) antennas which suffer from multipath loss and low penetration [1]. As a result, CP antennas are used in a variety of applications, including global navigation satellite systems, radar, radio frequency identification (RFID), and sensor systems [2]–[5]. In addition, CP antennas with multi-band coverage require fewer antenna components [6]–[9].

Furthermore, recent years have witnessed renewed interest in biconical antennas due to their straightforward design, ease of fabrication, and multiband coverage capability [10], [11]. In [12], wideband biconical antennas were proposed and experimented. A compact dual-band (1.575/2.45 GHz)

The associate editor coordinating the review of this manuscript and approving it for publication was Giorgio Montisci.

This work is licensed under a Creative Commons Attribution 4.0 License. For more information, see https://creativecommons.org/licenses/by/4.0/

LP/CP antenna scheme for outdoor/indoor applications in [13] was proposed, but it suffered from narrow impedance bandwidth (IBW). In [14], a dual-band (3.0/5.5 GHz) monopole antenna with frequency-selective surface-based corner reflector effectively achieved both frequency bands but failed to generate circular polarization. A dual-band (2.45/5.2 GHz) monopole antenna with multiple modified substrates for WLAN applications was proposed in [15]. Due to the standing wave current distribution along the longitudinal direction, the radiation pattern of conventional biconical antennas is thus of linear polarization [16].

As a result, a low-profile wideband CP circular patch antenna with two monopolar modes connected to a modified ground plane by conductive vias [17] was proposed to generate omnidirectional circular polarization. In [18], a patch antenna with vortex slots and shorting vias could achieve circular polarization. However, these CP antennas [17], [18] partially covered dual-band operating frequencies.

With the growing demand for dual-band CP antennas, a dual-band (2.45/5.80 GHz) antenna with adjustable stubs was proposed, and the antenna could achieve circular polarization but suffered from narrow axial ratio bandwidth (ARBW) in the lower-frequency band [19]. In [20], a dual-band (3.1/4.7 GHz) CP split-ring resonators with square slot was proposed, but it suffered from narrow ARBW. A dual-band CP planar monopole antenna in [21] could cover WLAN/Wi-Fi/Bluetooth/WiMAX frequency spectra but failed to achieve an omnidirectional radiation pattern.

Theoretically, an LP wave can be converted into a CP wave by using a wave polarizer [22], [23]. As a result, an omnidirectional CP antenna could be realized by incorporating a wave polarizer into an omnidirectional LP antenna. Specifically, this research proposes a novel dual-band (2.45/5.80 GHz) CP omnidirectional antenna scheme for WLAN applications by integrating a biconical radiating structure with a wave polarizer consisting of double-circular (inner and outer circles) parasitic parallelepiped elements. The biconical structure at the center is surrounded by double-circular parasitic parallelepiped elements which are uniformly and angularly arranged along the circumference of the biconical structure to convert an LP wave into a CP wave.

In this study, simulations were performed using CST Studio Suite and a prototype antenna was fabricated. Experiments were performed and results compared with the simulations. The performance metrics of the dual-band CP omnidirectional biconical antenna with double-circular parasitic parallelepiped elements included the impedance bandwidth ($|S_{11}| \leq -10$ dB), axial ratio (AR $\leq$ 3 dB), radiation pattern, and antenna gain. The research novelty is the application of a biconical radiating structure and double-circular parasitic parallelepiped elements to realizing circular polarization for dual-band WLAN applications.

This paper is organized as follows. Detailed antenna configurations are discussed in Section II. The parametric study is carried out in Section III. Simulated and measured results are presented in Section IV. Finally, conclusions are shown in Section V.

II. ANTENNA CONFIGURATION

Figure 1(a) shows the proposed biconical antenna with the half-angle of the bicone of θ_{hc}, where θ_{hc} is calculated from the impedance (Z_c) of an infinite biconical antenna (equation (1)).

$$Z_c = \frac{\eta}{\pi} \ln \cot \frac{\theta_{hc}}{2}, \tag{1}$$

where η is the impedance of free-space (=376.73 Ω) and θ_{hc} is the half-angle of the bicone. A half-angle of approximately 67° yields a 50 Ω match. Since infinitely long biconical elements are impossible to realize, the length of the bicone must be truncated. Given that the diameter of the biconical antenna is approximately one-wavelength (1.0λ) for the target lower-frequency band (2.40 GHz) [24], the height of the biconical antenna (H) is thus λ/2 of the lower-frequency band. In this research, the optimal parametric dimensions of the biconical antenna are as follows: $\theta_{hc} = 71°$, $H = 40$ mm, and $R_3 = 56$ mm.

Figure 1(b) shows the geometry of outer and inner parasitic parallelepiped elements functioning as the wave polarizer [22], [23] of the proposed CP biconical antenna scheme. The parallelepiped elements are of aluminum material.

Assuming an LP wave traveling in the x-direction with a 45° polarization relative to the positive y-axis, the electric field of the LP wave can be resolved into E_y and E_z components. Since the parasitic parallelepiped elements and air gap behave like a wave polarizer, the two electric field components (E_y and E_z) would travel at different speeds as the LP wave passes through the polarizer, resulting in a 90° phase difference.

By varying the outer and inner parallelepiped element thicknesses (d_1 and d_2), a 90° phase difference could be achieved, giving rise to circular polarization given that $|E_y| = |E_z|$. As a result, an omnidirectional CP antenna could be realized by angularly encircling an omnidirectional LP radiating source with a polarizer (i.e., double-circular parasitic parallelepiped elements).

In this research, the radiating source is a biconical structure of copper material. Since the electric field generated by the biconical structure is of vertical linear polarization, tilted parasitic parallelepiped elements were utilized to induce the polarizer effect (i.e., circular polarization).

Figure 1(b) illustrates the perspective view of the proposed dual-band CP omnidirectional biconical antenna scheme. Figure 1(c) shows the arrangement and displacement (from the center of the biconical structure) of the inner and outer parallelepiped elements around the biconical radiating structure. The parasitic parallelepiped elements are uniformly arranged along the circumference of the biconical structure with an angular interval of 360°/N, where N is the number of inner and outer parallelepiped elements. Figure 1(d)

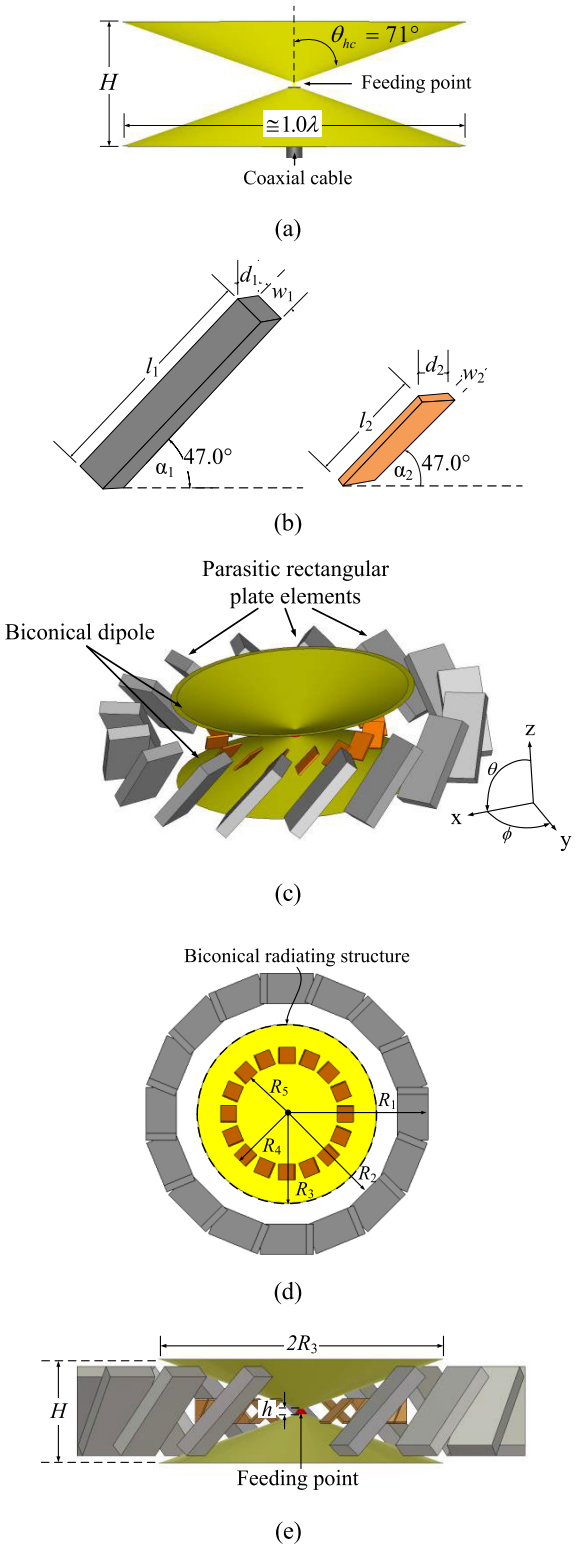

FIGURE 1. The proposed dual-band CP biconical antenna scheme: (a) biconical structure, (b) geometry of outer and inner parasitic parallelepiped elements, (c) perspective view, (d) arrangement of double-circular parallelepiped elements around the biconical structure, (e) front view.

shows the front view of the dual-band CP biconical antenna scheme with double-circular parallelepiped elements,

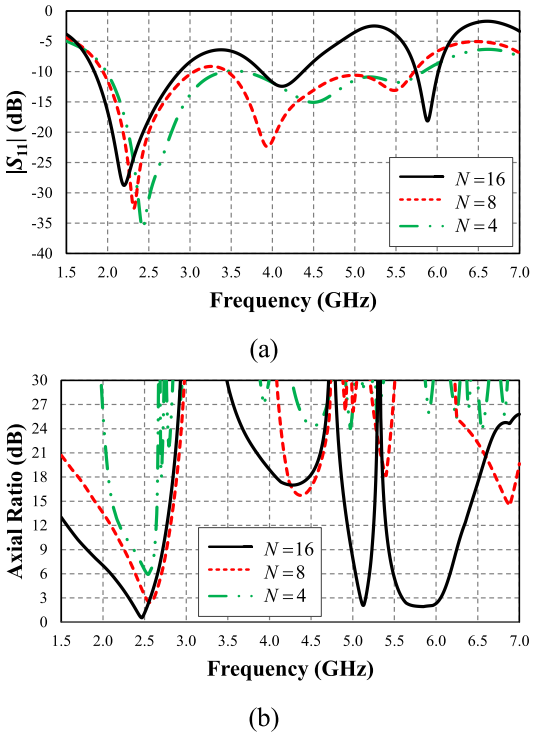

FIGURE 2. Simulated results of the dual-band CP biconical antenna scheme at $\theta = 90°$ under a variable number of inner and outer parallelepiped elements N: (a) $|S_{11}|$, (b) axial ratio.

with the feeding point at the contact point between the bicone.

III. PARAMETRIC STUDIES

To optimize the antenna parameters, simulations were performed using CST Studio Suite. In this study, the target lower- and upper-frequency bands of the dual-band CP antenna scheme were 2.40 – 2.485 and 5.725 – 5.875 GHz. Figures 2(a)-(b) show the simulated $|S_{11}|$ and axial ratio (AR) of the proposed dual-band CP biconical antenna scheme for different numbers (N) of inner and outer parasitic parallelepiped elements: 4, 8, and 16.

With $N = 4$ (i.e., the inner- and outer-circle parallelepiped elements were four each), the IBW ($|S_{11}| \leq -10$ dB) was 1.99 – 5.83 GHz, covering both lower- (2.45 GHz) and upper-frequency bands (5.80 GHz). The wide IBW could be attributed to limited number of inner- and outer-circle parasitic parallelepiped elements (i.e., $N = 4$ each). However, the AR was above 3dB (AR > 3 dB) for both lower- and upper-frequency bands.

With $N = 8$, the IBW was 1.95 – 3.04 GHz and 3.46 – 5.72 GHz for the lower- and upper-frequency bands, respectively. An impedance mismatch ($|S_{11}| > -10$dB) occurred in the upper-frequency band. The ARBW (AR ≤ 3 dB) was 3.90% at the lower-frequency band, covering 2.51 – 2.61 GHz. However, the AR was substantially larger than 3 dB (AR > 3 dB) for the upper-frequency band.

With $N = 16$, the IBWs and ARBWs of the lower-frequency band were 1.84 – 2.88 GHz and 2.31 – 2.57 GHz

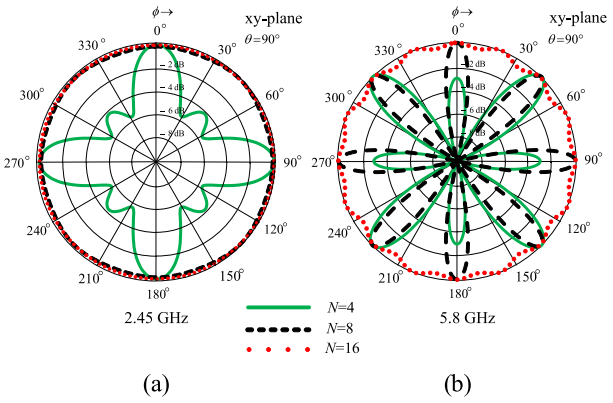

FIGURE 3. Simulated radiation patterns of the dual-band CP biconical antenna scheme at $\theta = 90°$ under variable N, where N is the number of inner and outer parallelepiped elements: (a) 2.45 GHz, (b) 5.80 GHz.

respectively, while those of the upper-frequency band were 5.72 – 6.01 GHz and 5.59 – 6.05 GHz respectively, achieving circular polarization for both bands.

Figures 3(a)-(b) illustrate the simulated radiation patterns of the proposed dual-band CP omnidirectional biconical antenna scheme at the center frequencies of 2.45 and 5.80 GHz respectively, for different numbers (N) of inner and outer parasitic parallelepiped elements: 4, 8, and 16.

With $N = 4$, the proposed biconical antenna scheme failed to achieve omnidirectional radiation pattern for both lower- and upper-frequency bands. With $N = 8$, the proposed antenna scheme achieved omnidirectional radiation pattern in the lower-frequency band, but the radiation pattern was non-omnidirectional in the upper-frequency band. With $N = 16$, the radiation patterns of the lower- and upper-frequency bands were omnidirectional. As a result, the optimal numbers of inner- and outer-circle parasitic parallelepiped elements (N) were 16 each.

Figure 4(a) shows the simulated $|S_{11}|$ and AR of the proposed dual-band CP biconical antenna scheme under different outer-circle parallelepiped widths (w_1): 4, 6, and 8 mm. With $w_1 = 4$ mm, the simulated IBWs ($|S_{11}| \leq -10$ dB) were 1.84 – 2.9 GHz and 5.6 – 5.94 GHz for the lower- and upper-frequency bands, respectively. The corresponding simulated ARBWs (AR $\leq$ 3 dB) were 2.36 – 2.54 GHz and 5.71 – 5.92 GHz.

With $w_1 = 6$ mm, the impedance matching remained relatively unchanged for the lower-frequency band, while that of the upper-frequency band deteriorated (from −30 dB to -18 dB). The 3-dB AR remained relatively unchanged for the lower-frequency band, while that of the upper-frequency band improved, resulting in wider ARBW (5.59 – 6.05 GHz).

With $w_1 = 8$ mm, the impedance matching of lower-frequency band significantly improved ($|S_{11}| < -30$dB), while that of the upper-frequency band deteriorated and failed to cover the target upper-frequency band. The 3-dB AR remained relatively unchanged for the lower-frequency band, while that of the upper-frequency band deteriorated (AR > 3 dB), with ARBW partially covering the upper-frequency band (5.56 – 5.72 GHz). As a result, the optimal w_1 was 6 mm.

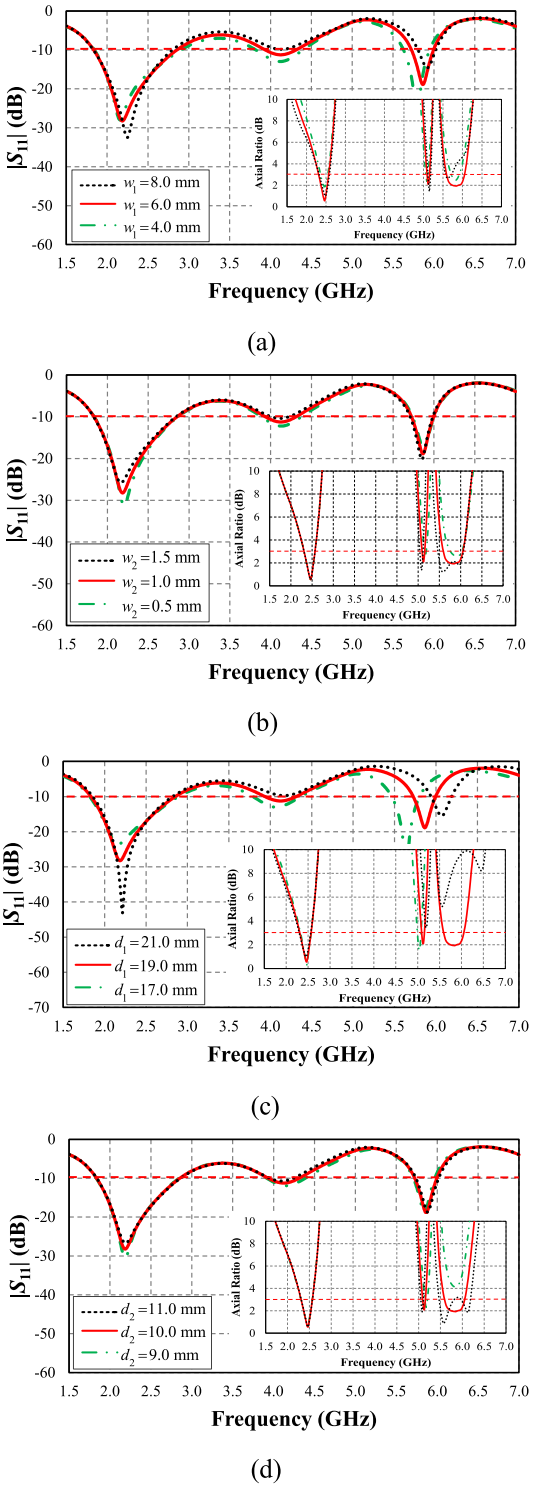

FIGURE 4. Effects of parameters on $|S_{11}|$ and axial ratio: (a) w_1, (b) w_2, (c) d_1, (d) d_2.

Figure 4(a) shows the simulated $|S_{11}|$ and AR of the proposed dual-band CP biconical antenna scheme under different outer-circle parallelepiped widths (w_1): 4, 6, and 8 mm. In comparison with $w_1 = 4$ mm, given $w_1 = 6$ mm,

the impedance matching remained relatively unchanged for the lower-frequency band, while that of the upper-frequency band deteriorated. The AR remained relatively unchanged for the lower-frequency band, while that of the upper-frequency band improved, resulting in wider ARBW.

With $w_1 = 8$ mm, the impedance matching of lower-frequency band significantly improved, while that of the upper-frequency band deteriorated and failed to cover the target upper-frequency band. The AR remained relatively unchanged for the lower-frequency band, while that of the upper-frequency band deteriorated, with ARBW partially covering the upper-frequency band. As a result, the optimal w_1 was 6 mm.

Figure 4(b) shows the simulated $|S_{11}|$ and AR of the proposed antenna scheme under variable inner-circle parallelepiped widths (w_2): 0.5, 1, and 1.5 mm. The simulated results were almost identical to those of w_1 (Figure 4(a)), and the optimal w_2 was 1 mm.

Figure 4(c) shows the simulated $|S_{11}|$ and AR under different outer-circle parallelepiped thickness (d_1): 17, 19, and 21 mm. With $d_1 = 17$ mm, the AR of the upper-frequency band was excessively high, failing to achieve circular polarization. With $d_1 = 19$ mm, the impedance matching slightly improved for the lower-frequency band ($|S_{11}| = -28$ dB), while that of the upper-frequency band deteriorated. The AR were below 3 dB for both lower- and upper-frequency bands. With $d_1 = 21$ mm, the impedance matching of the lower-frequency band significantly improved ($|S_{11}| < -43$ dB), while that of the upper-frequency band deteriorated and shifted to higher frequency, failing to cover the target upper-frequency band. The AR remained relatively unchanged for the lower-frequency band, while that of the upper-frequency band noticeably deteriorated, with ARBW failing to cover the target upper-frequency band. The optimal d_1 was thus 19 mm.

Figure 4(d) illustrates the simulated $|S_{11}|$ and AR under variable inner-circle parallelepiped thickness (d_2): 9, 10, and 11 mm. The results showed that varying d_2 had minimal impact on the impedance matching of the proposed antenna scheme. Meanwhile, varying d_2 minimally affected the AR of the lower-frequency band, vis-à-vis that of the upper-frequency band. The optimal d_2 was 9 mm since the ARBW covered the target dual-band frequencies.

Figures 5(a)-(b) show the simulated $|S_{11}|$ and AR under variable outer-circle parallelepiped element lengths (l_1): 0, 15, 25, 42, and 62 mm. In Figure 5(a), with $l_1 = 0$ mm, the impedance matching was achieved at 2.7 GHz and 4.4 GHz, which were outside the target dual-band frequencies (2.45/5.80 GHz). The impedance matching improved and moved closer to the target frequencies as l_1 increased from 15 mm to 42 mm. An impedance mismatch occurred when $l_1 = 62$ mm.

In Figure 5(b), with $l_1 = 0$, 15, and 25 mm, AR was above 3dB for both lower- and upper-frequency bands. With $l_1 = 62$ mm, AR was higher than 3 dB in the upper-frequency band. Thus, the optimal l_1 was 42 mm as AR was below 3 dB for both lower- and upper-frequency bands.

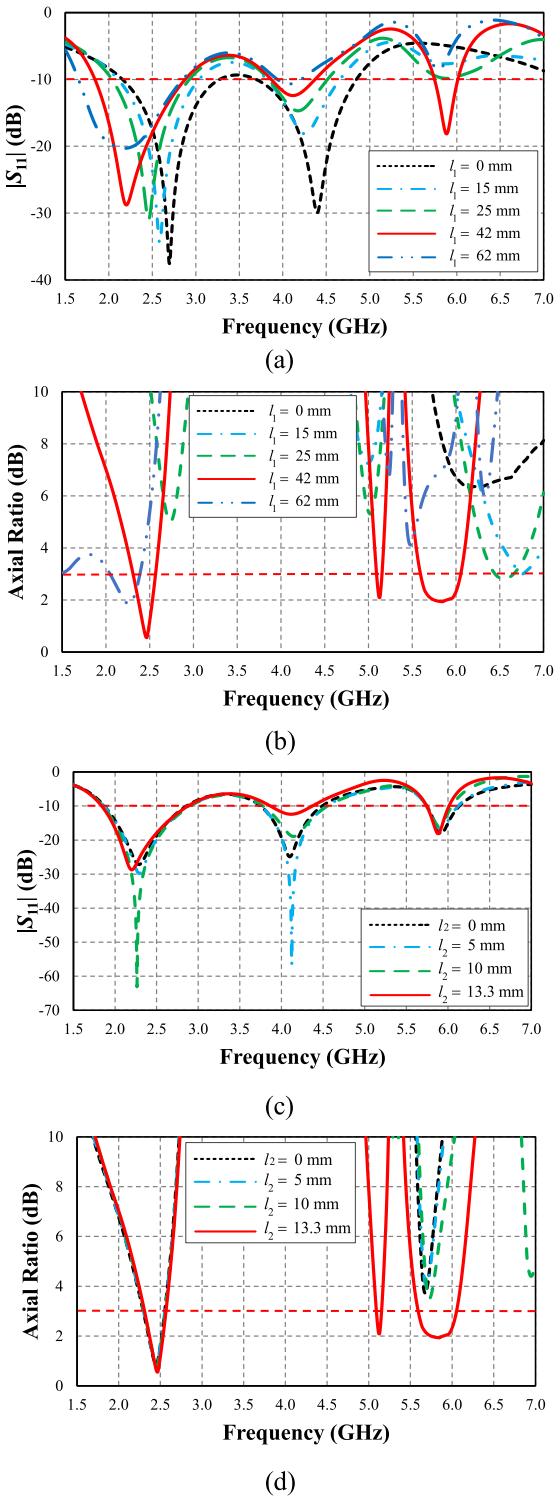

FIGURE 5. Effects of parameters on $|S_{11}|$: (a) l_1, (b) l_1 on AR, (c) l_2 on $|S_{11}|$, (d) l_2 on AR.

Figures 5(c)-(d) illustrate the simulated $|S_{11}|$ and AR under variable inner-circle parallelepiped element lengths (l_2): 0, 5, 10, and 13.3 mm. In Figure 5(c), except for $l_2 = 10$ mm

in the lower-frequency band, varying l_2 had minimal impact on the impedance matching of the proposed antenna scheme. In Figure 5(d), varying l_2 had minimal impact on the AR in the lower-frequency band, while the AR of the upper-frequency band improved as l_2 increased. The optimal l_2 was 13.3 mm as the IBW and ARBW covered both lower- and upper-frequency bands.

Figure 6(a) shows the simulated $|S_{11}|$ and AR of the proposed dual-band CP biconical antenna scheme under variable biconical height (H): 38.5, 40.5, and 42.5 mm. With $H = 38.5$ mm, the IBW for the lower- and upper-frequency bands covered 1.84 – 2.93 GHz and 5.87 – 6.08 GHz. The IBW for the upper-frequency band failed to cover the target upper-frequency band. With $H = 40.5$ and 42.5 mm, the IBW covered both target frequency bands.

Meanwhile, given $H = 38.5$ mm, the ARBW covered 2.37 – 2.57 GHz, while that for the upper-frequency band of 5.12 – 5.3 GHz was far below the target frequency band. With $H = 40.5$ mm, the AR was below 3 dB for both the target lower- and upper-frequency bands. However, with $H = 42.5$ mm, the AR of the upper-frequency band was well above 3 dB, failing to achieving circular polarization. The optimal H was thus 40.5 mm.

Figure 6(b) shows the simulated $|S_{11}|$ and AR under different displacements of outer-circle parallelepiped elements (R_1): 88, 90, and 92 mm, where R_1 is the radius between the outermost edge and the center. With $R_1 = 88$ mm, the IBW for the lower- and upper-frequency bands covered 1.87 – 2.83 GHz and 5.94 – 6.22 GHz. With $R_1 = 90$ mm, the IBW covered both the target lower- and upper-frequency bands. However, the IBW for the upper-frequency band covered 5.05 – 5.81 GHz for $R_1 = 92$ mm, partially covering the target upper-frequency band.

Meanwhile, with $R_1 = 88$ mm, the ARBW of 2.29 – 2.55 GHz covered the target lower-frequency band, while that of the upper-frequency band of 5.51 – 5.62 GHz was below the target frequency band. With $R_1 = 90$ mm, the AR was below 3 dB for both the target lower- and upper-frequency bands. With $R_1 = 92$ mm, the AR of the upper-frequency band was well above 3 dB, failing to achieve circular polarization. As a result, the optimal R_1 was 90 mm.

Figure 6(c) shows the simulated $|S_{11}|$ and AR under different displacements of inner-circle parallelepiped elements (R_4): 30.5, 31.5, and 32.5 mm. R_4 is the radius from the center to the outer edge of the inner-circle parallelepiped elements. The results showed that R_4 had minimal effect on the impedance matching of the proposed dual-band CP antenna scheme. The AR for the lower-frequency band was below 3 dB, independent of R_4. For the upper-frequency band, with $R_4 = 30.5$ mm, the AR was above 3 dB. For $R_4 = 31.5$ mm, the ARBW covered the target upper-frequency band. With $R_4 = 32.5$ mm, the ARBW were outside of the target frequency band. The optimal R_4 was thus 31.5 mm.

Figure 6(d) depicts the simulated $|S_{11}|$ and AR under variable radii of the biconical structure (R_3): 53, 56, and 59 mm. The impedance matching improved with increase in R_3, but $|S_{11}|$ shifted to lower frequency as R_3 increased.

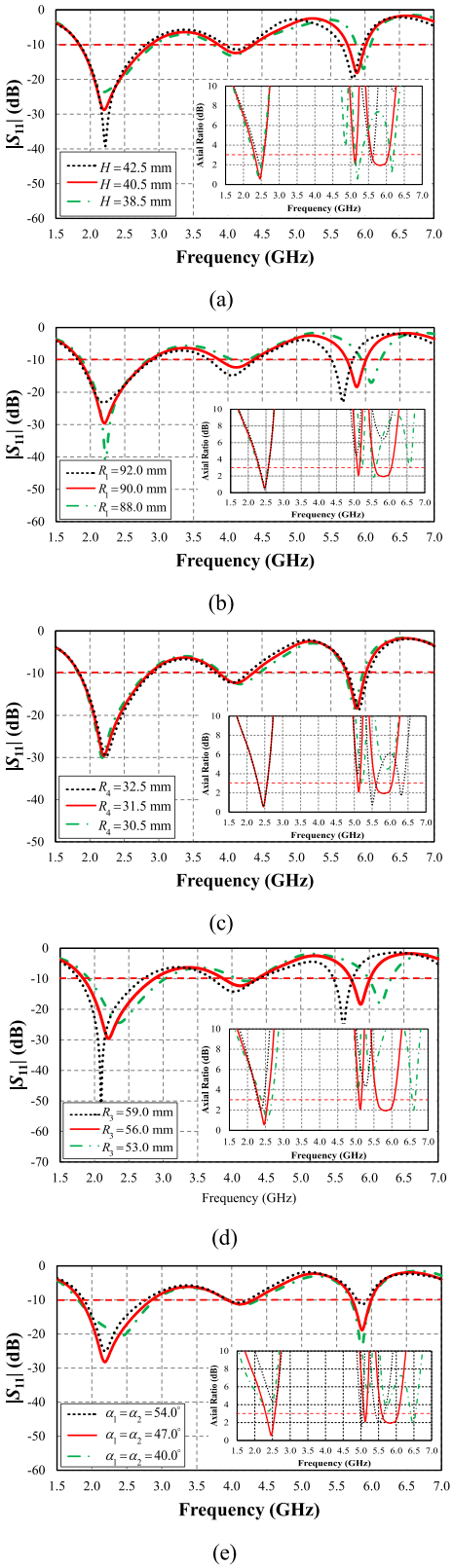

FIGURE 6. Effects of parameters on $|S_{11}|$ and axial ratio: (a) H, (b) R_1, (c) R_4, (d) R_3, (e) α_1, α_2.

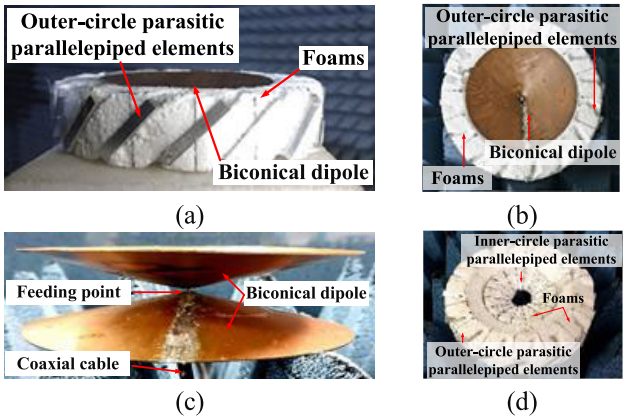

FIGURE 7. Prototype of the proposed dual-band (2.45/5.80 GHz) CP omnidirectional biconical antenna scheme: (a) perspective view, (b) top view, (c) biconical structure, (d) geometry of outer and inner parasitic parallelepiped elements.

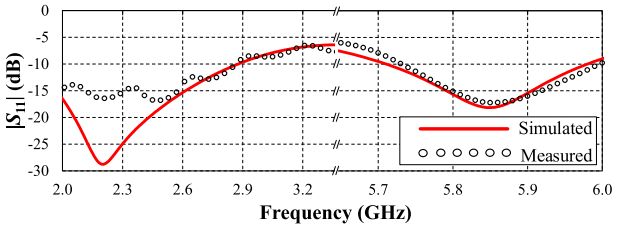

FIGURE 8. Simulated and measured $|S_{11}|$ of the proposed dual-band CP omnidirectional biconical antenna.

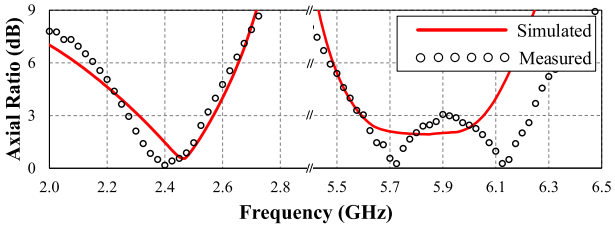

FIGURE 9. Simulated and measured AR of the proposed dual-band CP omnidirectional biconical antenna.

For the upper-frequency band, the IBW, given $R_3 = 53$ and 59 mm, failed to cover the target frequency band. With $R_3 = 56$ mm, the IBW covered both target frequency bands. The AR for the upper-frequency band, given $R_3 = 53$ and 59 mm, were well above 3 dB. Meanwhile, with $R_3 = 56$ mm, the ARBW covered the target upper-frequency band. The optimal R_3 was 56 mm.

Figure 6(e) shows the simulated $|S_{11}|$ and AR under different angles of the outer- and inner-circle parallelepiped elements (α_1, α_2): 40°, 47°, and 54°. The impedance matching for the lower-frequency band generally improved with increase in α_1 and α_2, but that for the upper-frequency band deteriorated as α_1 and α_2 increased. The AR for the lower-frequency band was below 3 dB, independent of α_1 and α_2.

For the upper-frequency band, with α_1, $\alpha_2 = 40°$, the ARBW partially covered the target frequency band. For α_1, $\alpha_2 = 47°$, the ARBW covered the target upper-frequency band. The proposed antenna scheme achieved wider ARBW with α_1, $\alpha_2 = 54°$, but the IBW failed to cover the target upper-frequency band. The optimal α_1 and α_2 were thus 47°.

The parametric studies indicate that the position, size and tilt angle of the parasitic parallelepiped elements play a crucial role in the LP-to-CP conversion and the antenna performance, including the impedance and AR bandwidths, omnidirectionality, and gain. Specifically, the size of the parasitic parallelepiped elements (i.e., d_1, d_2, l_1, and l_2) affect the AR bandwidth. Meanwhile, the position (R_1 and R_4) and the tilt angles (α_1 and α_2) of the parasitic parallelepiped elements affect the IBW and AR bandwidths and omnidirectionality. Besides, non-uniform distances between the parasitic elements also result in non-omnidirectional radition pattern in the xy plane. By comparison, at 5.8 GHz, the impedance and AR bandwidths are more sensitive to the arrangement of inner parasitic parallelepiped elements, vis-à-vis at 2.4 GHz

IV. SIMULATED AND MEASURED RESULTS

To verify, a dual-band CP omnidirectional biconical antenna prototype was fabricated and experiments conducted. Figure 7(a) depicts the prototype of the proposed dual-band CP omnidirectional biconical antenna with double-circular parasitic parallelepiped elements. Figure 7(b) shows the top view of the antenna prototype where the outer and inner parasitic elements were arranged around the biconical antenna. In the antenna prototype, closed-cell extruded polystyrene foam (i.e., Styrofoam) was used as the divider between the parasitic elements with a tilt angle of 47°. The dielectric constant of Styrofoam ($\varepsilon_r = 1.1$) is close to that of air ($\varepsilon_r = 1.0006$) [25].

Fig. 7(c) shows the biconical antenna structure, consisting of welded tapered copper sheets of 1 mm in thickness each. The biconical antenna is fed by a coaxial cable at the center of the structure. Fig. 7(d) shows the outer and inner parasitic elements (without the biconical structure) with Styrofoam between the parasitic elements. The $|S_{11}|$, AR, radiation pattern, and antenna gain were measured using an HP8520C network analyzer in an anechoic chamber. The ETS-Lindgren Model 3100 Series Conical Log Spiral antennas were used to verify left-hand circular polarized (LHCP) and right-hand circular polarized (RHCP) radiations.

Figure 8 compares the simulated and measured $|S_{11}|$ of the proposed dual-band (2.45/5.80 GHz) CP omnidirectional biconical antenna. The simulated IBWs ($|S_{11}| \leq -10$ dB) were 1.84 – 2.88 GHz and 5.71 – 5.98 GHz for the lower- and upper-frequency bands. The corresponding measured IBWs were 1.84 – 2.89 GHz and 5.73 – 5.99 GHz. The simulated and measured IBWs were agreeable in spite of comparably inferior measured impedance matching in the lower-frequency band. The inferiority could be attributed to the antenna fabrication.

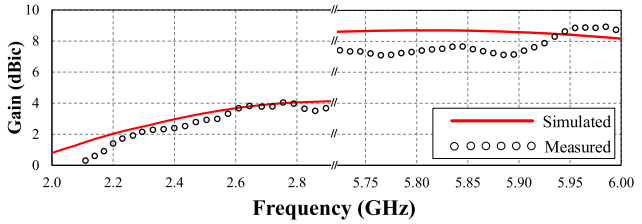

FIGURE 10. Simulated and measured gains of the proposed dual-band CP omnidirectional biconical antenna.

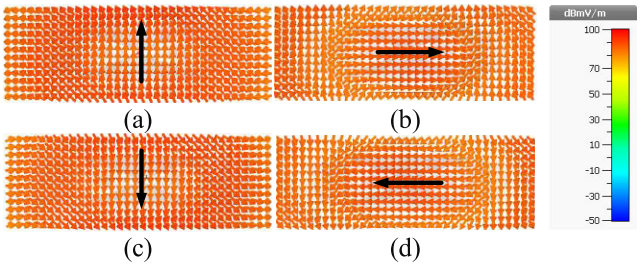

FIGURE 11. Simulated electric field at 2.45 GHz of the proposed CP biconical antenna (front view) at: (a) $t = 0$, (b) $t = T/4$, (c) $t = T/2$, (d) $t = 3T/4$.

Figure 9 compares the simulated and measured ARs of the dual-band CP omnidirectional biconical antenna scheme at $\theta = 90°$. The simulated ARBWs (AR $\leq$ 3dB) were 2.31 – 2.57 GHz) and 5.60 – 6.05 GHz for the lower- and upper-frequency bands respectively, while the corresponding measured ARBWs were 2.27 – 2.54 GHz and 5.60 – 6.22 GHz. The simulated and measured results were reasonably agreeable, with discrepancies in the upper-frequency band attributable to non-uniformity of the parallelepiped element angles (α_1, α_2) and displacements (R_2 and R_5) along the biconical circumference during the antenna fabrication. In this research, there were 16 parasitic parallelepiped elements each for inner and outer circles.

Figure 10 illustrates the simulated and measured antenna maximum gains at the lower-frequency and upper-frequency bands of the dual-band CP omnidirectional biconical antenna scheme. The simulated and measured gains were agreeable. The measured antenna gains were higher than 2.3 dBic for both the lower- and upper-frequency bands, with the maximum gains of 3.2 dBic and 8.5 dBic at the center frequencies of the lower- (2.45 GHz) and upper-frequency (5.80 GHz) bands. The slightly lower measured gains were attributable to the antenna fabrication.

Figures 11(a)-(d) illustrate the simulated electric field of the proposed CP omnidirectional biconical antenna scheme (front view) at 2.45 GHz at $t = 0$, $T/4$, $T/2$, and $3T/4$, respectively. At $t = 0$, the electric field flowed upward, and at $t = T/4$, the electric field shifted 90° and traveled rightward. At $t = T/2$, the electric field flowed downward, with a 90° phase shift vis-à-vis at $t = T/4$. At $t = 3T/4$, the direction of the electric field was leftward. The electric field of the proposed CP omnidirectional biconical antenna scheme rotated counterclockwise (i.e., LHCP).

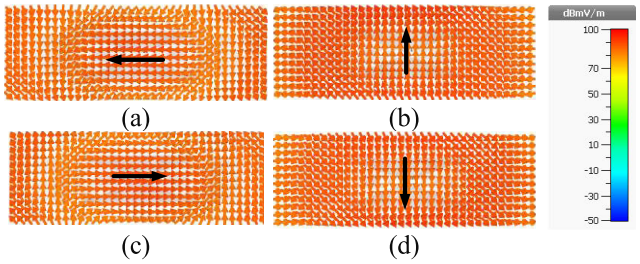

FIGURE 12. Simulated electric field at 5.80 GHz of the proposed CP biconical antenna (front view) at: (a) $t = 0$, (b) $t = T/4$, (c) $t = T/2$, (d) $t = 3T/4$.

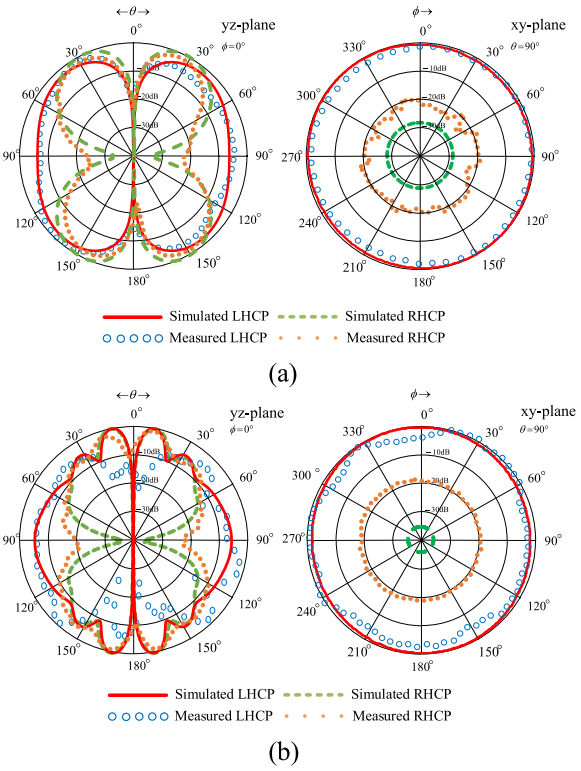

FIGURE 13. Simulated and measured radiation patterns in the yz- and xy-planes of the dual-band CP biconical antenna with double-circular parallelepiped elements at: (a) 2.45 GHz, (b) 5.80 GHz.

Figures 12(a)-(d) show the simulated electric field of the proposed CP omnidirectional biconical antenna scheme (front view) at 5.80 GHz at $t = 0$, $T/4$, $T/2$, and $3T/4$, respectively. At $t = 0$, the electric field traveled leftward, and at $t = T/4$, the electric field traveled upward. At $t = T/2$, the electric field flowed rightward, with a 90° phase shift vis-à-vis at $t = T/4$. At $t = 3T/4$, the direction of the electric field was downward. The electric field of the proposed CP omnidirectional biconical antenna scheme is of LHCP.

At 5.80 GHz, the HPBWs of the simulated and measured LHCP radiation patterns in the yz-plane were 80° and 80° respectively, as shown in Figure 13(b) on the left-hand side. The simulated and measured radiation patterns were reasonably agreeable. the XPL was around 20 dB. In Figure 13(b) on the right-hand side, the simulated and

TABLE 1. Optimal parameters of the proposed dual-band CP omnidirectional biconical antenna with double-circular parasitic parallelepiped elements.

Parameter	N	H	h	R_1	R_2	R_3	R_4	R_5
Value	16	40.5 mm	1.0 mm	90.0 mm	71.0 mm	56.0 mm	31.5 mm	21.5 mm
Parameter	w_1	w_2	d_1	d_2	l_1	l_2	α_1	α_2
Value	6.0 mm	1.0 mm	19.0 mm	10.0 mm	42.0 mm	13.3 mm	47°	47°

TABLE 2. The antenna parameters, IBW and ARBW of existing studies and this current research.

Reference	$f_{c\ (IBW)}$ (GHz)	$f_{c\ (ARBW)}$ (GHz)	Maximum Gain	IBW (%)	ARBW (%)	Electrical dimension at λ_L	Radiation Pattern	Proposed antenna/technology
[13]	1.575 2.45	1.575 -	5.10 dBic 5.03 dBi	1.837 0.735	0.699 -	0.68×0.68×0.053	Unidirectional	A pentagonal patch with CSRR and U-shape slot radiator adjoining AMC ground plane
[15]	2.45 5.2	-	3.04 dBi 2.60 dBi	25.24 18.18	-	0.56×0.53×0.039	Bidirectional	Monopole antenna with five-layer suspended substrates
[17]	2.45	2.45	4.68 dBic	19.8	17.7	1.34×1.34×0.0024	Omnidirectional	Two monopolar modes of a circular radiating patch connected to curved-branch ground plane using conductive vias
[18]	2.845	2.885	1.0 dBic	51.7	57.9	0.63×0.63×0.101	Omnidirectional	Three resonant modes with disc-loaded coaxial probe, six shorting vias, and a circular patch with six vortex slots
[19]	2.5 5.80	2.41 5.38	2.0 dBic 4.5 dBic	17.39 52.63	1.68 13.50	0.35×0.25×0.0067	Bidirectional	Semi-circle printed monopole fed by microstrip with complementary metal structure connected to the ground plane
[20]	3.1 4.7	3.1 4.75	5.9 dBic 6.2 dBic	13.15 13.62	3.2 4.2	0.66×0.66×0.1287	Unidirectional	Microstrip line fed slot antenna with split-ring resonators (SRRs)
[21]	2.565 5.215	2.085 5.575	1.4 dBic 4.5 dBic	14.42 44.67	22.63 15.24	0.34×0.38×0.0127	Bidirectional	L-shaped monopole, an inverted-L strip, and a modified ground
Proposed Antenna	2.36 5.845	2.44 5.93	3.2 dBic 8.5 dBic	44.44 4.56	11.22 10.49	1.10×1.10×0.248	Omnidirectional	Biconical radiating structure with double-circular (inner and outer) parasitic parallelepiped elements encircling the biconical structure

λ_L: the free-space wavelength corresponding to the lowest operating frequency of the antenna.

measured radiation patterns in the xy-plane were of LHCP omnidirectionality, and the XPL was around 20 dB.

Table 2 compares the parameters and performance of the existing antenna schemes and the proposed dual-band CP omnidirectional biconical antenna with double-circular parasitic parallelepiped elements. Specifically, despite more compact than the proposed antenna scheme, the planar, low-profile, dual-band and dual-polarized antenna in [13] yields unidirectional pattern with single-band circular polarization. Besides, the impedance and AR bandwidths are narrower than those of the proposed antenna scheme. In [15], although smaller in size, the substrate-integrated suspended line high-efficiency monopole antenna radiates bidirectional pattern in dual-frequency band.

In [17] and [18], the CP omnidirectional antennas achieve wider impedance and AR bandwidths, but the antennas can radiate in single-frequency band with antenna lower gain than the proposed antenna scheme. Despite smaller in size and wider impedance bandwidth, the antenna in [19] has bidirectional radiation.

In [20], although smaller, the dual-band CP split ring resonators loaded square slot antenna fails to achieve omnidirectional radiation pattern, with narrow AR bandwidth. In [21], the dual-band CP planar monopole antenna has not radiated omnidirectionally despite smaller in size.

By comparison, the proposed antenna scheme can achieve circularly polarized omnidirectionality in dual-frequency band (2.45/5.80 GHz) in spite of the larger electrical dimension.

V. CONCLUSION

This research proposed a novel dual-band 2.45/5.80 GHz CP omnidirectional biconical antenna with double-circular parasitic parallelepiped elements for WLAN applications. In the antenna development, the double-circular (inner and outer circles) parasitic parallelepiped elements were uniformly and angularly arranged surrounding the biconical radiating structure, and the double-circular parallelepiped elements functioned as a wave polarizer that converts LP omnidirectional electric fields from the biconical radiating structure into omnidirectional CP fields. The target lower- and upper-frequency bands of the proposed dual-band CP omnidirectional antenna scheme were 2.4 – 2.485 and 5.725 – 5.875 GHz. In the study, simulations were performed to optimize the antenna parameters, and an antenna prototype was fabricated and experiments were conducted. The simulated IBWs were 44.0% (1.84 – 2.88 GHz) and 4.62% (5.71 – 5.98 GHz) for the lower- and upper-frequency bands, respectively. The corresponding measured IBWs were 44.4% (1.84 – 2.89 GHz) and 4.56% (5.73 – 5.99 GHz). The simulated ARBWs were 10.65% (2.31 – 2.57 GHz) and 7.73% (5.6 – 6.05 GHz), while the measured ARBWs were 11.22% (2.27 – 2.54 GHz) and 10.49% (5.6 – 6.2 GHz), respectively. The simulated and measured radiation patterns of the proposed CP biconical antenna scheme were LHCP omnidirectional, with the measured antenna gains of 3.2 dBic and 8.5 dBic at 2.45 and 5.80 GHz, respectively. Despite the narrow IBW (4.56%) and ARBW (10.49%) for the upper-frequency band, the bandwidths adequately covered the target upper frequency band (5.725 – 5.875 GHz), rendering the proposed CP omnidirectional biconical antenna scheme operationally suitable for WLAN applications. Nonetheless, to address the narrow IBW, subsequent research would experiment with different geometries of the radiating structure (i.e., different structures other than the biconical). In addition, to tackle the relatively narrow ARBW, future research would experimentally vary the dimensions and angles of the inner- and outer-circle parasitic parallelepiped elements. The material of the parallelepiped elements could also be altered from aluminum to dielectric resonator materials to realize wider ARBW.

REFERENCES

[1] S. Gao, Q. Luo, and F. Zhu, *Circularly Polarized Antenna*. Hoboken, NJ, USA: Wiley, 2014.

[2] K. K. So, H. Wong, K. M. Luk, and C. H. Chan, "Miniaturized circularly polarized patch antenna with low back radiation for GPS satellite communications," *IEEE Trans. Antennas Propag.*, vol. 63, no. 12, pp. 5934–5938, Dec. 2015.

[3] Nasimuddin, X. Qing, and Z. N. Chen, "A compact circularly polarized slotted patch antenna for GNSS applications," *IEEE Trans. Antennas Propag.*, vol. 62, no. 12, pp. 6506–6509, Dec. 2014.

[4] Y.-F. Lin, C.-H. Lee, S.-C. Pan, and H.-M. Chen, "Proximity-fed circularly polarized slotted patch antenna for RFID handheld reader," *IEEE Trans. Antennas Propag.*, vol. 61, no. 10, pp. 5283–5286, Oct. 2013.

[5] B. Rana and S. K. Parui, "Microstrip line fed wideband circularly-polarized dielectric resonator antenna array for microwave image sensing," *IEEE Sensors Lett.*, vol. 1, no. 3, pp. 1–4, Jun. 2017.

[6] P. Mousavi, "Multiband multipolarization integrated monopole slots antenna for vehicular telematics applications," *IEEE Trans. Antennas Propag.*, vol. 59, no. 8, pp. 3123–3127, Aug. 2011.

[7] W. Hu, Y.-Z. Yin, X. Yang, and P. Fei, "Compact multiresonator-loaded planar antenna for multiband operation," *IEEE Trans. Antennas Propag.*, vol. 61, no. 5, pp. 2838–2841, May 2013.

[8] K.-C. Lin, C.-H. Lin, and Y.-C. Lin, "Simple printed multiband antenna with novel parasitic-element design for multistandard mobile phone applications," *IEEE Trans. Antennas Propag.*, vol. 61, no. 1, pp. 488–491, Jan. 2013.

[9] A. Boukarkar, X. Q. Lin, Y. Jiang, and Y. Q. Yu, "Miniaturized single-feed multiband patch antennas," *IEEE Trans. Antennas Propag.*, vol. 65, no. 2, pp. 850–854, Feb. 2017.

[10] S. Liao, P. Chen, and Q. Xue, "Ka-band omnidirectional high gain stacked dual bicone antenna," *IEEE Trans. Antennas Propag.*, vol. 64, no. 1, pp. 294–299, Jan. 2016.

[11] F. E. S. Pereira and M. H. C. Dias, "A case study on the bandwidth broadening of a skeletal biconical antenna," *IEEE Latin Amer. Trans.*, vol. 16, no. 8, pp. 294–299, Aug. 2018.

[12] N. Rostomyan, A. T. Ott, M. D. Blech, R. Brem, C. J. Eisner, and T. F. Eibert, "A balanced impulse radiating omnidirectional ultrawideband stacked biconical antenna," *IEEE Trans. Antennas Propag.*, vol. 63, no. 1, pp. 59–68, Jan. 2015.

[13] K. N. Paracha, S. K. L. A. Rahim, P. J. Soh, M. R. Kamarudin, Y. C. Lo, and M. T. Islam, "A low profile, dual-band, dual polarized antenna for indoor/outdoor wearable application," *IEEE Access*, vol. 7, pp. 33277–33288, 2019.

[14] A. Chatterjee and S. K. Parui, "Performance enhancement of a dual-band monopole antenna by using a frequency-selective surface-based corner reflector," *IEEE Trans. Antennas Propag.*, vol. 64, no. 6, pp. 59–68, Jun. 2016.

[15] Y. He, K. Ma, N. Yan, and H. Zhang, "Dual-band monopole antenna using substrate-integrated suspended line technology for WLAN application," *IEEE Antennas Wireless Propag. Lett.*, vol. 16, pp. 2776–2779, 2017.

[16] C. A. Balanis, *Antenna Theory-Analysis and Design*, 3rd ed. Hoboken, NJ, USA: Wiley, 2005.

[17] Y. M. Pan, S. Y. Zheng, and B. J. Hu, "Wideband and low-profile omnidirectional circularly polarized patch antenna," *IEEE Trans. Antennas Propag.*, vol. 62, no. 8, pp. 4347–4351, Aug. 2014.

[18] D. Yu, S. X. Gong, Y. T. Wan, Y. L. Yao, Y. X. Xu, and F. W. Wang, "Wideband omnidirectional circularly polarized patch antenna based on vortex slots and shorting vias," *IEEE Trans. Antennas Propag.*, vol. 62, no. 8, pp. 3970–3977, Aug. 2014.

[19] W. Liang, Y. C. Jiao, Y. Luan, and C. Tian, "A dual-band circularly polarized complementary antenna," *IEEE Antennas Wireless Propag. Lett.*, vol. 14, pp. 1153–1156, 2015.

[20] K. Kandasamy, B. Majumder, J. Mukherjee, and K. P. Ray, "Dual-band circularly polarized split ring resonators loaded square slot antenna," *IEEE Trans. Antennas Propag.*, vol. 64, no. 8, pp. 3640–3645, Aug. 2016.

[21] Q. Li, Y. Wei, C. Ding, M. Tan, L. Zhang, X. Lei, G. Wu, Z. Wang, Z. Lu, and Y. Gong, "Dual-band circularly polarised planar monopole antenna for WLAN/Wi-Fi/Bluetooth/WiMAX applications," *IET Microw., Antennas Propag.*, vol. 12, no. 6, pp. 972–976, Mar. 2018.

[22] J. D. Kraus, *Antennas*, 2nd ed. New York, NY, USA: McGraw-Hill, 1988.

[23] R. C. Johnson and H. Jasik, *Antenna Engineering Handbook*. New York, NY, USA: McGraw-Hill, 1961.

[24] H. G. Schantz, *The Art and Science of Ultrawideband Antennas*, 2nd ed. Boston, MA, USA: Artech House, 2015.

[25] S. W. Ellingson, *Electromagnetics*, 2nd ed. Blacksburg, VA, USA: Virginia Tech Publishing, 2020.

PISIT JANPANGNGERN was born in Lampang, Thailand, in 1991. He received the B.Eng. degree from the Rajamangala University of Technology Thanyaburi, Thailand, in 2015, and the M.Eng. degree from the King Mongkut's Institute of Technology Ladkrabang (KMITL), Thailand, in 2017, where he is currently pursuing the D.Eng. degree. His research interest includes omnidirectional circularly polarized antennas.

DANAI TORRUNGRUENG (Senior Member, IEEE) received the B.Eng. degree in electrical engineering from Chulalongkorn University, Bangkok, Thailand, in 1993, and the M.S. and Ph.D. degrees in electrical engineering from The Ohio State University, Columbus, OH, USA, in 1996 and 2000, respectively. From 1995 to 2000, he was a Graduate Research Assistant (GRA) with the ElectroScience Laboratory, Department of Electrical Engineering, The Ohio State University. Prior to joining Asian University, Thailand, in 2002, he worked as a Senior Engineer in the USA, involved in research and development of the urban propagation modeling project. He is currently a Professor with the Department of Teacher Training in Electrical Engineering, Faculty of Technical Education, King Mongkut's University of Technology North Bangkok, Bangkok. Furthermore, he is also a Co-Founder of the Innovative Electromagnetics Academy of Thailand (iEMAT) founded, in 2013. From 2004 to 2009, he invented generalized Smith charts, called T-charts or Meta-Smith charts, for solving several problems associated with conjugately characteristic-impedance transmission lines (CCITLs) and bi-characteristic-impedance transmission lines (BCITLs), including their useful applications in applied electromagnetics. He authored *MetaSmith Charts and Their Potential Applications* (Morgan & Claypool, 2010) and *Advanced Transmission Line Modeling in Electromagnetics* (Charansanitwong Printing, 2012). His research interests include electromagnetic sensors, fast computational electromagnetics, rough surface scattering, propagation modeling, electromagnetic wave theory, and microwave theory and techniques and antennas. He is also a member of the ECTI, where he had served as the ECTI Technical Chair for electromagnetics, from 2014 to 2017. In addition, he served as the TPC Co-Chair for TJMW2016, the Vice Co-Chair for TJMW2017, and the TPC Chair for ISAP2017. In 2000, he won the Award in the National URSI Student Paper Competition at the 2000 National Radio Science Meeting in Boulder, CO, USA.

MONAI KRAIRIKSH (Senior Member, IEEE) was born in Bangkok, Thailand. He received the B.Eng., M.Eng., and D.Eng. degrees in electrical engineering from the King Mongkut's Institute of Technology Ladkrabang (KMITL), Thailand, in 1981, 1984, and 1994, respectively. He was a Visiting Research Scholar at Tokai University, in 1988, and at Yokosuka Radio Communications Research Center, Communications Research Laboratory (CRL), in 2004. He worked as the Director of the Research Center for Communications and Information Technology, from 1997 to 2002. He joined the KMITL and is currently a Professor at the Department of Telecommunication Engineering. His main research interests include antennas for wireless communications and microwave in agricultural applications. He was the Chairperson of the IEEE MTT/AP/Ed Joint Chapter, in 2005 and 2006. He served as the General Chairperson of the 2007 Asia-Pacific Microwave Conference, and the Advisory Committee of the 2009 International Symposium on Antennas and Propagation. He was the President of the Electrical Engineering/Electronics, Computer, Telecommunications and Information Technology Association (ECTI), in 2010 and 2011, and was the Editor-in-Chief of the *ECTI Transactions on Electrical Engineering, Electronics, and Communications*. He was recognized as a Senior Research Scholar of the Thailand Research Fund in 2005 and 2008 and a Distinguished Research Scholar of the National Research Council of Thailand. He served as a Distinguished Lecturer for the IEEE Antennas and Propagation Society, during 2012–2014.

CHUWONG PHONGCHAROENPANICH (Member, IEEE) received the B.Eng. (Hons.), M.Eng., and D.Eng. degrees from the King Mongkut's Institute of Technology Ladkrabang (KMITL), Bangkok, Thailand, in 1996, 1998, and 2001, respectively. He is currently a Professor with the Department of Telecommunications Engineering, KMITL, where he also works as the Leader of the Innovative Antenna and Electromagnetic Applications Research Laboratory. His research interests include antenna design for various mobile and wireless communications, conformal antennas, and array antenna theory. He is also a Senior Member of IEICE and a member of ECTI. He has served as the Chair for the IEEE MTT/AP/ED Thailand Chapter, from 2014 to 2018. He has been on organizing committee of several international conferences, including the TPC Chair of 2009 International Symposium on Antennas and Propagation (ISAP 2009) and a TPC member of ISAP 2012. He is also a Reviewer of many scientific journals, including the IEEE TRANSACTIONS ON ANTENNAS AND PROPAGATION, IEEE ACCESS, *IET Microwaves, Antennas and Propagation*, *Electronics Letters*, and *ECTI Transactions*, and many international conferences, including ISAP and APMC. He was on the Board Committee of the ECTI Association, from 2008 to 2011 and 2014 to 2015. He was an Associate Editor of the *IEICE Transactions on Communications* and the *ECTI Transactions on Electrical Engineering, Electronics, and Communications*. He is also an Associate Editor of the *IEICE Communications Express*.